Two- and three-layered composite scintillators based on the Ce^{3+} doped GAGG and TbAG garnets for simultaneous registration of various types of ionizing radiation

[1,2]Y. Syrotych*, [1]V. Gorbenko, [3]R. Kucerkova, [3]J.A. Mares, [3]M. Nikl, [4]K. Kamada, [4]A. Yoshikawa, A. Fedorov[5], O. Sidleskiy[6], [7,8]J. Winiecki, [1,8]Yu. Zorenko

[1]Department of Physics of Kazimierz Wielki University in Bydgoszcz, 85090 Bydgoszcz, Poland

[2]Department of Mechatronics, Kazimierz Wielki University in Bydgoszcz, 85074 Bydgoszcz, Poland

[3]Institute of Physics, Academy of Sciences of Czech Republic, 16200 Prague, Czech Republic

[4]Institute for Materials Research, Tohoku University, Sendai 980-8577, Japan

[5]Institute of Single Crystals, National Academy of Sciences of Ukraine, 61001 Kharkiv, Ukraine

[6]Institute for Scintillation Materials, National Academy of Sciences of Ukraine, 61001 Kharkiv, Ukraine

[7]Medical Physics Department of Oncology Center, Bydgoszcz, 85796 Bydgoszcz, Poland

[8]Oncology and Brachytherapy Department of Collegium Medicum of Nicolaus Copernicus University, 85067 Bydgoszcz, Poland

Abstract. This work presents our most recent results in the development of composite scintillators using Liquid Phase Epitaxy growth method, based on the single crystalline films and single crystals of garnet compounds for radiation monitoring of different components of mixed ionization radiation fluxes. Such composite scintillators present two and three layered epitaxial structures consisting of two single crystalline films of Ce^{3+} doped garnets, namely $Gd_3Al_{5-x}Ga_xO_{12}$:Ce garnet with Ga content x=1.75–2.25 as a first film layer and $Tb_3Al_5O_{12}$:Ce garnet as a second film layer. As substrates, the $Gd_3Al_{5-x}Ga_xO_{12}$:Ce single crystals with fixed Ga concentration x=2.3, 2.5 and 3.0 were used. For estimation of scintillation properties of the respective epitaxial structures (pulse height spectra, light yield and scintillation decay kinetics) we have used three types of ionizing radiation: α–particles (^{239}Pu), β-particles (^{90}Sr + ^{90}Y) and γ–quanta (^{137}Cs).

Keywords: Liquid Phase Epitaxy, composite scintillators, single crystalline films, radiation monitoring, mixed ionization radiation.

1. Introduction

The development of composite scintillators using the liquid phase epitaxy (LPE) growth method is an important step in the future evolution of the so-called *"phoswich-type"* radiation detectors for different applications [1-6]. The LPE grown composite scintillators can be applied for simultaneous recording and analysis of various components of mixed ionizing radiation, which includes particles and photons with

different penetration depths [1-10]. Using the LPE method, during the last ten years large efforts were done to create different types of two layered (film and crystal) composite scintillators based on the single crystalline films (SCFs) and single crystals (SCs) of various oxide compounds including garnets, tungstates, perovskites and ortho- and pyrosilicates [1-10]. Furthermore, the composite scintillating screens based on the SCFs of heavy garnets, perovskites and orthosilicates were created for application in the microimaging technique with micrometer spatial resolution [11, 12]. We have also succeeded in the development of doubly layered epitaxial structures based on the garnets and perovskites for simultaneous detection of various components of mixed radiation fluxes using different thermostimulated properties of film and substrate materials [13-16]. Therefore, the LPE technique is currently indicated as very flexible technology for the growth of multilayer composite luminescent materials for different optoelectronic devices [10, 17,18].

Application of the LPE technique for the composite scintillators growth enables the creation of epitaxial structures containing the films and substrates with different lattice constants, dopants and thicknesses. More specifically, it concerns the use of epitaxial structures with one or two SCF scintillators dedicated to record short-range α-particles and middle-range β-particles as well as the thick enough substrates intended for registration of deep-penetrating X- and gamma-ray radiations [10]. The substrate for optimal composite scintillator for detecting high-energy β-particles and γ-quanta should have high density $\boldsymbol{\rho}$ and effective atomic number $\boldsymbol{Z_{eff}}$**.** For this reason, we considered in our previous work heavy scintillators such as $CdWO_4$ (CWO) tungstate, $Lu_3Al_5O_{12}$ (LuAG) and $Gd_3Al_2Ga_2O_{12}$:Ce (GAGG) garnets, as well as Lu_2SiO_5 (LSO) orthosilicates and $(La,Gd)_2Si_2O_7$ (LGPS) pyrosilicates with high $\boldsymbol{\rho}$ and $\boldsymbol{Z_{eff}}$ values as promising candidates for substrates [1-6, 10].

An ideal composite scintillator for detecting high-energy α- and β-particles and γ-quanta must contain a substrate with high ρ and Z_{eff} values and a lattice constant suitable for performance of the LPE growth of film scintillators. For this reason, the $Gd_3Al_2Ga_3O_{12}$:Ce garnet with large density ρ=6.5 g/cm^3 and an effective atomic number Z_{eff}=54.4, is one of such materials in which we are interested as a part of composite scintillator [9]. Notably, these crystals show a relatively high light yield of ~50,000 photons per MeV^{-1} and an energy resolution of 4.5–4.8% at 662 keV γ-rays excitation (^{137}Cs source) [19] and are related to the top of the best scintillators for radiation monitoring and medical applications. Among the later application, it is worth mentioning CT and PET diagnostics, as well as the possibility of using GAGG:Ce scintillators for in-situ measurement of radiation dose in the brachytherapy procedure with ^{192}Ir or other gamma sources. Moreover, the composite scintillators based on GAGG:Ce and other garnets are good candidates for the development of composite detectors for measuring the radiation dose of α-particles, ^{7}Li ions and γ-rays components in the quantum range of the boron-capture-neutron therapy (BNCT) procedure.

The family of $Gd_3Al_{5-x}Ga_xO_{12}$:Ce ($GAGG_x$:Ce) garnet crystals can be synthesized in the narrow range of gallium concentrations **x**, ranging from x=2.3 to 3.0 formula units. Such a narrow range of Ga content in the crystals arises from the incongruent melting and crystallization processes, causing single-phase and homogeneous $GAGG_x$:Ce crystals growth only in the x=2.3-3 range. From the other hand, these structural features of $GAGG_x$:Ce crystals with different gallium concentrations x can be used also for the production of diverse types of composite scintillators [10, 21, 22]. In the context of creation composite scintillators, the GAGG:Ce SC substrates stands out as an excellent material for growing different types of SCF scintillators using LPE method. It is noteworthy that increasing the Ga content from x=2.3 to 3.0 in $GAGG_x$:Ce crystals results in a slight decrease in light yield (LY) but significantly accelerates the scintillation response [9, 10]. This property allows the use of substrates with variable scintillation decays at the development of composite scintillators on their base.

Taking into account the mentioned properties of the $GAGG_x$:Ce SC substrates, it makes sense to grow SCF scintillators based on another garnets on these substrates in so-called *quasi-homoepitaxial mode* of the LPE growth. This approach enables the separation of signals originating from various sources of ionizing radiation with different penetration abilities. The first suitable material for this purpose is $Tb_3Al_5O_{12}$:Ce (TbAG:Ce) garnet, which has a scintillation decay profile different from that of $GAGG_x$:Ce garnet [8]. However, due to a substantial difference in lattice constants between these materials, being equal approximately to 1.6% at x=3 [23], the growth of a buffer transition layer (from 15 up even to 100 μm) based on the $GAGG_x$:Ce SCFs with a lower than x=2.3 gallium concentration was performed. This approach facilitates the alignment of the lattice constants, enabling the growth of a TbAG:Ce SCF onto $GAGG_x$:Ce SC substrates with any Ga content x.

The current study is based on our group's previous efforts in developing promising composite scintillators using epitaxial structures of garnet compounds [10, 24]. In particular, this paper presents our new achievements on the fabrication of two- and three-layered composite scintillators based on TbAG:Ce and $GAGG_{1.75-2.25}$:Ce SCFs grown by LPE method onto $GAGG_x$:Ce (x=2.3-3) SC substrates for radiation monitoring and medical applications.

2. Samples and experimental technique

The composite scintillators preparation for this study was performed in several stages. The initial stage involved producing $GAGG_x$:Ce SC substrates, where x=2.3, 2.5 and 3.0 with nominal Ce^{3+} content of 0.1 at.%. The crystals of these garnets were synthesized using the Czochralski method in IMR Tohoku University, Japan and ISMA, Ukraine. As it has been mentioned previously, the growth of these crystals is

restricted by the amount of gallium in the solid solution, which varies between 2.3 and 3 formula units. However, there is a method that allows to significantly expand the range of Ga concentrations in the GAGGx:Ce garnet structure. Such a method is crystallization of these materials from super-cooled melt solution using the LPE method, which enables growing $GAGG_x$:Ce SCFs with x in a wide range x=0-5 [25].

The Ce^{3+}-doped $GAGG_x$:Ce SCFs (x=1.75, 2, 2.25) were grown onto three types of $GAGG_x$:Ce SC substrates with different Ga content x=2.3, 2.5 and 3.0 using the LPE technique at the Physical Faculty of UKW in Bydgoszcz, Poland (Fig. 1, Table 1). The melt solution for the growth of SCF scintillators was prepared on the base of conventional $PbO\text{-}B_2O_3$ flux. Since these films were initially employed to minimize the lattice mismatch between the $GAGG_x$:Ce substrate and the TbAG:Ce SCFs, we consider the $GAGG_x$:Ce SCFs as a *transition layer*. The thickness of such a layers was reaching from 15 up to 20 μm, and from 38 to 105 μm for creation of two-layered and three layered epitaxial structures, respectively (Table 1).

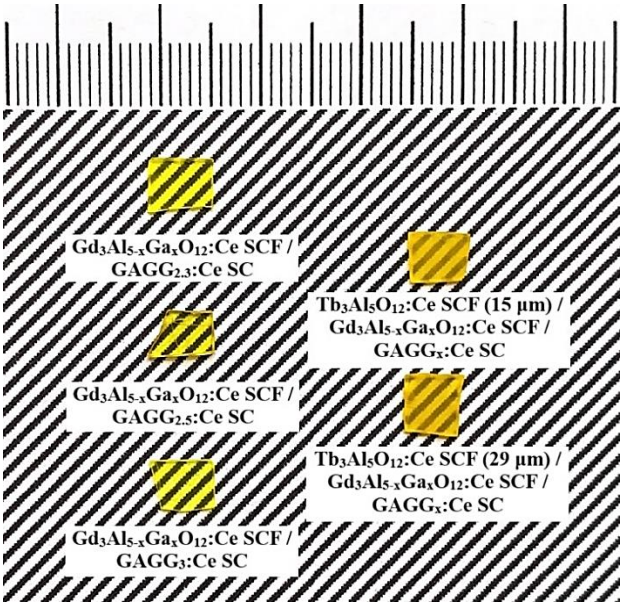

Fig. 1. Photo of $GAGG_x$:Ce SCF_1/$GAGG_x$:Ce SC and TbAG:Ce SCF_2/$GAGG_x$:Ce SCF_1/$GAGG_x$:Ce SC composite scintillators with different Ga concentration and film's thicknesses.

Table 1. The content, thickness, lattice constants of $GAGG_x$:Ce SC (x=2.3, 2.5, 3) substrates; $GAGG_x$:Ce SCF_1 (x=1.75, 2, 2.25) and TbAG:Ce SCF_2 as well as SCF_2/SCF_1/SC substrate misfits $\mathbf{m = (a_{SCF} - a_{Sub})/ a_{Sub} * 100\ \%}$ of the respective epitaxial structures.

N	Samples	SCF_2/SCF_1/ SC substrate thickness, μm	Lattice constant, a, Å	m, %
1	$GAGG_3$:Ce	500	12.220	-
2	$GAGG_{2.5}$:Ce	500	12.231	-
3	$GAGG_{2.3}$:Ce	500	12.259	-
4	$GAGG_2$:Ce SCF_1 / $GAGG_3$:Ce SC	18/500	12.192	- 0.23 %

5	$GAGG_{2.25}$:Ce SCF_1 / $GAGG_{2.5}$:Ce	15/500	12.216	- 0.12 %
6	$GAGG_{1.75}$:Ce SCF_1 / $GAGG_{2.3}$:Ce SC	20/500	12.204	- 0.45 %
7	TbAG:Ce SCF_2/ $GAGG_2$:Ce SCF_1/$GAGG_3$:Ce SC	15/105/500	12.076	-1.05 %
8	TbAG:Ce SCF_2/$GAGG_{1.75}$:Ce SCF_1/$GAGG_3$:Ce SC	29/38/500	12. 072	- 0.98%

The next stage of the process was the growth of TbAG:Ce SCF_2 of various thicknesses in the range of 25-30 μm, onto two-layered $GAGG_x$:Ce SCF_1/$GAGG_3$:Ce SC epitaxial structures (Table 1). The TbAG:Ce SCF_2 thickness in mentioned range is considered sufficient for the full absorption of α-particles in the mixed ionization fluxes. The variations in the SCFs thickness provide also the flexibility for choosing the most optimal option for the successful simultaneous detection of α-, β- particles and γ-quanta using different scintillation layers of composite scintillators.

For this study, it is important to note that there are specific discrepancies in the chemical composition of the films. During the growth process, it is essential to consider the segregation coefficient of ions, which, in the case of $GAGG_x$:Ce SCF_1, significantly differs between the real and nominal composition of the compound [26, 27]. Specifically, for the SCF compositions with a nominal Ga content of 3.0, 3.25 and 3.5 in the melt solution, the average segregation coefficient of Ga ions is 0.58, 0.62 and 0.65, respectively [28]. Therefore, we can assume that the approximate compositions of the SCFs are equivalent to $Gd_3Al_{3.25}Ga_{1.75}O_{12}$:Ce ($GAGG_{1.75}$:Ce), $Gd_3Al_3Ga_2O_{12}$:Ce ($GAGG_2$:Ce) and $Gd_3Al_{2.75}Ga_{2.25}O_{12}$:Ce ($GAGG_{2.25}$:Ce), respectively. Henceforth, this designation will be used below. However, the Ce^{3+} concentration in these $GAGG_x$:Ce SCF_1 and TbAG:Ce SCF_3 samples was close to 0.1 at. % with deviation ± 10%, depending slightly on the melt content and SCF growth temperature and growth rate.

The XRD measurements (spectrometer DRON 4, X-ray source) were used for characterization of the structural quality of $GAGG_x$:Ce SC substrates with Ga content x=2.3; 2.5 and 3 (Fig.2a); the $GAGG_x$:Ce SCF_1, where x=1.75; 2 and 2.25 (Fig.2b), and finally TbAG:Ce SCF_2 (Fig.3c). We have also calculated the lattice constant **a** of SCF samples and the misfit between the lattice constants of SCFs and $GAGG_x$:Ce substrates $\mathbf{m= (a_{SCF} - a_{Sub})/a_{Sub}*100\ \%}$. As can be seen from Figs. 2a, 2b and Table 1), the lattice constant of the GAGGx:Ce SC and GAGGx:Ce SCF1 substrates gradually increased when the x value varies from x = 2.5 to 3.0 and from x = 1.75 to 2.25, respectively. The SCF/substrate misfit is also depend on Ga content x in substrates and SCFs (x_{sub} and x_{SCF}, respectively) and increased from **m=** - 0.12 % for x_{SCF}/x_{sub}= 1.75/2.3 to **m**= - 0.45 % for x_{SCF}/x_{sub}=2.25/2.5 (Table 1).

Furthermore, the TbAG:Ce SCF_2 has a much smaller lattice constant, than $GAGG_x$:Ce SCF_1 (x=2-2.25) "substrates", which explains such a large **m**= - 0.98% / -1.05 % misfit of lattice constants of respective garnets (Table 1). Interesting, that lattice constant TbAG:Ce SCF grown onto SCF with Ga content x=2 little bit larger than in counterpart grown onto SCF with less Ga concentration x=1.75 most

likely due to the slightly different growth conditions and higher content of large-sized Pb^{2+} flux admixture in the first SCF sample with extremely high thickness (105 μm).

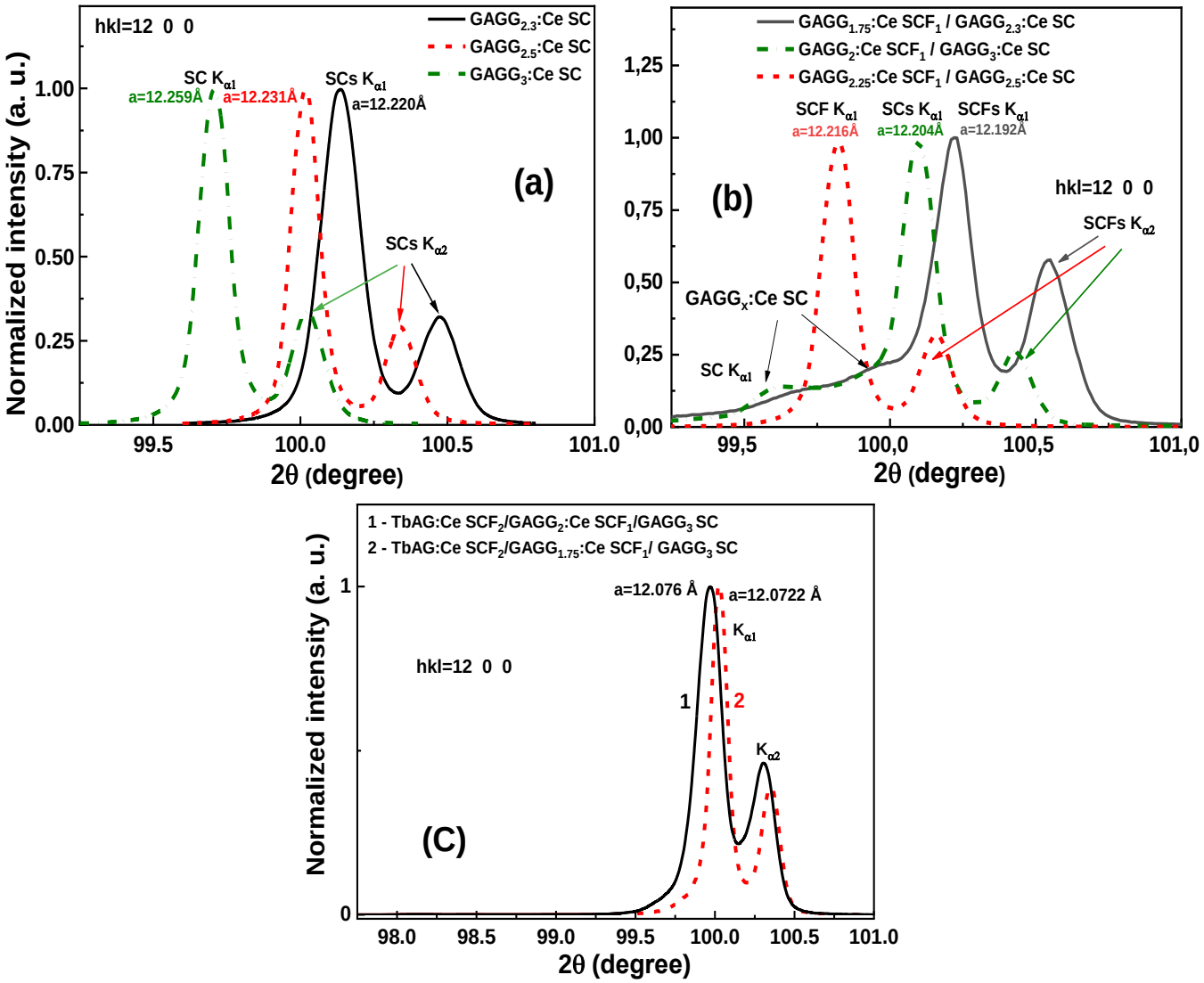

Fig. 2. XRD patterns of $GAGG_x$:Ce SC (x=2.3, 2.5 and 3) substrates; (a); two layered $GAGG_x$:Ce SCF_1/$GAGG_x$:Ce SC (b) and three-layered TbAG:Ce SCF_2/ $GAGG_{1.75-2}$:Ce SCF_1/$GAGG_3$:Ce SC epitaxial structures (c).

It is worth noting that reflections from the $GAGG_x$:Ce substrates were also recorded in some film samples, namely in $GAGG_{1.75}$:Ce SCF_1/$GAGG_{2.3}$:Ce SC and $GAGG_2$:Ce SCF_1/$GAGG_3$:Ce SC epitaxial structures due to their relatively small thickness in the 15-20 μm range (Fig.2b). This is also observed for the TbAG:Ce SCF_2/$GAGG_{1.75-2}O_{12}$:Ce SCF_1/$GAGG_3$:Ce SC composites, although the intensity of these reflexes is two-three time smaller and not observed in Fig.2c.

For characterization of the luminescent and scintillation properties of SCF and bulk SC parts of composite scintillators, the absorption spectra, cathodoluminescence (CL) spectra, pulse height spectra (PHS), light yield (LY) and scintillation decay kinetics under excitation by α– (^{239}Pu), β- (^{90}Sr) particles and γ–rays (^{137}Cs) were measured for two selected groups of two- and three-layered composite scintillators: $GAGG_{1.75\text{-}2.25}$:Ce SCF_1/$GAGG_{2.3\text{-}3}$:Ce SC (type I) with a SCF_1 thickness of 15-20 μm; and TbAG:Ce SCF_2/ $GAGG_{1.75\text{-}2}$:Ce SCF_1/$GAGG_3$:Ce SC (Type II) with a SCF_1 and SCF_2 thickness of 39-105 μm and 15-29 μm, respectively (see Table 1). The absorption spectra were measured using a Jasco 760 UV-Vis spectrometer within the 200 to 1100 nm wavelength range. CL spectra measurements of both SCF and SC samples were conducted using a JEOL JSM-820 scanning electron microscope with an electron beam energy of 20 kV using Stellar Net grating spectrometer equipped with CCD camera. Initial measurements of scintillation LY and decay kinetics for SCF parts of composite scintillators were performed at Physical Faculty of UKW in Bydgoszcz using a setup consisted of a Hamamatsu H6521 photomultiplier, multichannel analyzer, Tektronix TDS3052 digital oscilloscope, and selected YAG:Ce SCF as a reference sample. Subsequently, PHS measurements for these composite scintillators were performed at the Institute of Physics, Czech Academy of Science in Prague using a setup on the base of a hybrid PMT (HPMT DEP PP0475B with preamplifier), measuring electronics (Ortec 672 Spectroscopy Amplifier and 927 ASPEC MCA), and PC control. The SCF and SC substrate samples were excited using α-particles from ^{239}Pu source with an energy of 5.15 MeV, β-particles from ^{90}Sr source (546 keV) and γ-quanta from ^{137}Cs source (661.7 keV). All measurements were conducted at room temperature (RT).

3. Results and discussion

Absorption spectra. The absorption spectra of two layered $GAGG_{1.75\text{-}2.25}$:Ce SCF_1/$GAGG_{2.3\text{-}3}$:Ce SC composite scintillators (three samples) and three-layered TbAG:Ce SCF_2/ $GAGG_{1.75\text{-}2}$:Ce SCF_1/ $GAGG_3$:Ce SC (two samples) composite scintillators are compared with the spectra of $GAGG_x$:Ce SC substrates (x=2.3-3) in Fig. 3. The distinct bands peaked at 275 and 313-315 nm in the spectra of all $GAGG_x$:Ce substrates and SCF_1 can be attributed to the $^8S_{7/2}\rightarrow{}^6I_{3/2\text{-}7/2}$ and $^8S_{7/2}\rightarrow{}^6P_{3/2\text{-}7/2}$ transitions of Gd^{3+} ions, respectively [29].

The absorption spectra of TbAG:Ce SCF_2/ $GAGG_{1.75\text{-}2}$:Ce SCF_1/$GAGG_3$:Ce SC composite scintillator samples containing Tb^{3+} and Gd^{3+} ions reveal the lines corresponding to these cations. Specifically, the bands centered around ~270 nm belong to the low spin-allowed (LS) $4f\rightarrow5d_2$ and $4f\rightarrow5d_1$ absorption transitions of Tb^{3+} ions. Also, the low intensity peaks positioned at 372-377 nm range can be attributed to the $^7F_0\rightarrow{}^5D_3$ f-f transitions of Tb^{3+} ions [30].

The 4f-5d (^{2}E) transitions of Ce^{3+} ions are responsible for the absorption bands within the 338-342 nm and 438-451 nm ranges (designated as E_2 and E_1 bands, respectively) for the samples of doubly- and triply layered composite scintillators, as well as $GAGG_x$:Ce SC substrates. Other Ce^{3+} absorption bands in these scintillators are situated below 230 nm and associated with the 4f-5d(T_{2g}) transitions [31, 32].

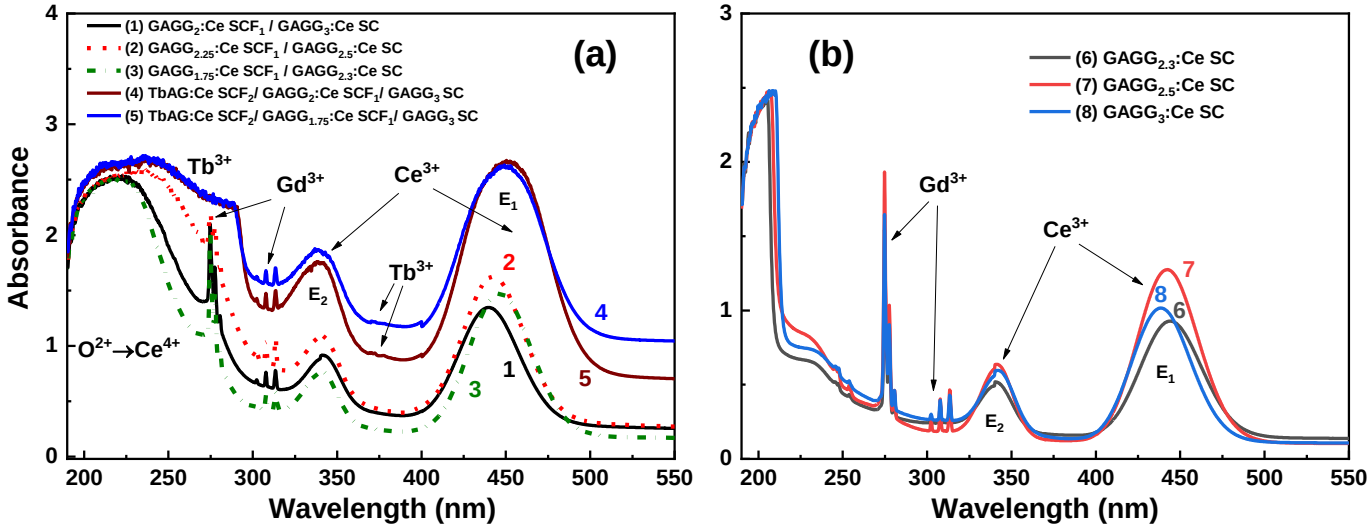

Fig.3. Absorption spectra of two layered $GAGG_{1.75\text{-}2.25}$:Ce SCF_1 / $GAGG_{2.3\text{-}3}$:Ce SC (1-3) and three-layered TbAG:Ce SCF_2/ $GAGG_{1.75\text{-}2}$:Ce SCF_1/ $GAGG_3$:Ce SC composite scintillators (4, 5), in comparison with absorption spectra of $GAGG_x$:Ce (x=2.3-3) substrates (6-8).

As can be seen in Fig. 3, the absorption spectra of composite scintillators, grown from a PbO-based flux, exhibit the additional broad band peaking around at 255 nm. This band is not observed in the absorption spectra of $GAGG_x$:Ce SC substrates, and its intensity is strongly dependent on the SCF thickness. The presence of this band is associated with the $O^{2-}\rightarrow Ce^{4+}$ charge transfer transitions (CTTs) in TbAG:Ce and $GAGG_x$:Ce SCFs components of composited scintillators. This phenomenon is analogous to the formation of such bands in crystals and films doped with two-charged A^{2+} ions (where A=Mg, Ca, Ba, Sr), such as YAG:Ce, LuAG:Ce, and GAGG:Ce crystals and films [33-35].

The creation of the Ce^{4+} state in the studied SCFs is attributed to the incorporation of Pb^{2+} impurities during the LPE growth process with using PbO-based fluxes. The formation of the Ce^{4+} state is energetically favorable for the local charge and volume compensation of the Pb^{2+} excess in SCFs of various oxides grown from PbO flux [26]. It is noteworthy that the absorption band of Gd^{3+} ions strongly overlaps with the broad $O^{2+}\rightarrow Ce^{4+}$ absorption bands peaking at 255 nm [33-35].

Cathodoluminescence (CL) spectra. The normalized RT CL spectra of $GAGG_{x.}$:Ce (x=2.3-3) SC substrates in comparison with two types of composite scintillators based on the two-layered $GAGG_{1.75\text{-}}$

$_{2.25}$:Ce SCF$_1$/GAGG$_x$:Ce SC (x=2.3-3) epitaxial structures and three layered TbAG:Ce SCFs/GAGG$_{1.75-2}$:Ce SCFs/GAGG$_3$:Ce SC epitaxial structures with different SCF thickness are shown in Fig. 4.

Using the CL spectra, valuable information can be obtained about the luminescent properties of Ce^{3+} ions in various garnet hosts depending on the material composition. The CL spectra of GAGG$_x$:Ce (x=2.3, 3.5, 3) SC substrates exhibit emission bands peaking in the 544-554 nm range (Fig.4). These bands

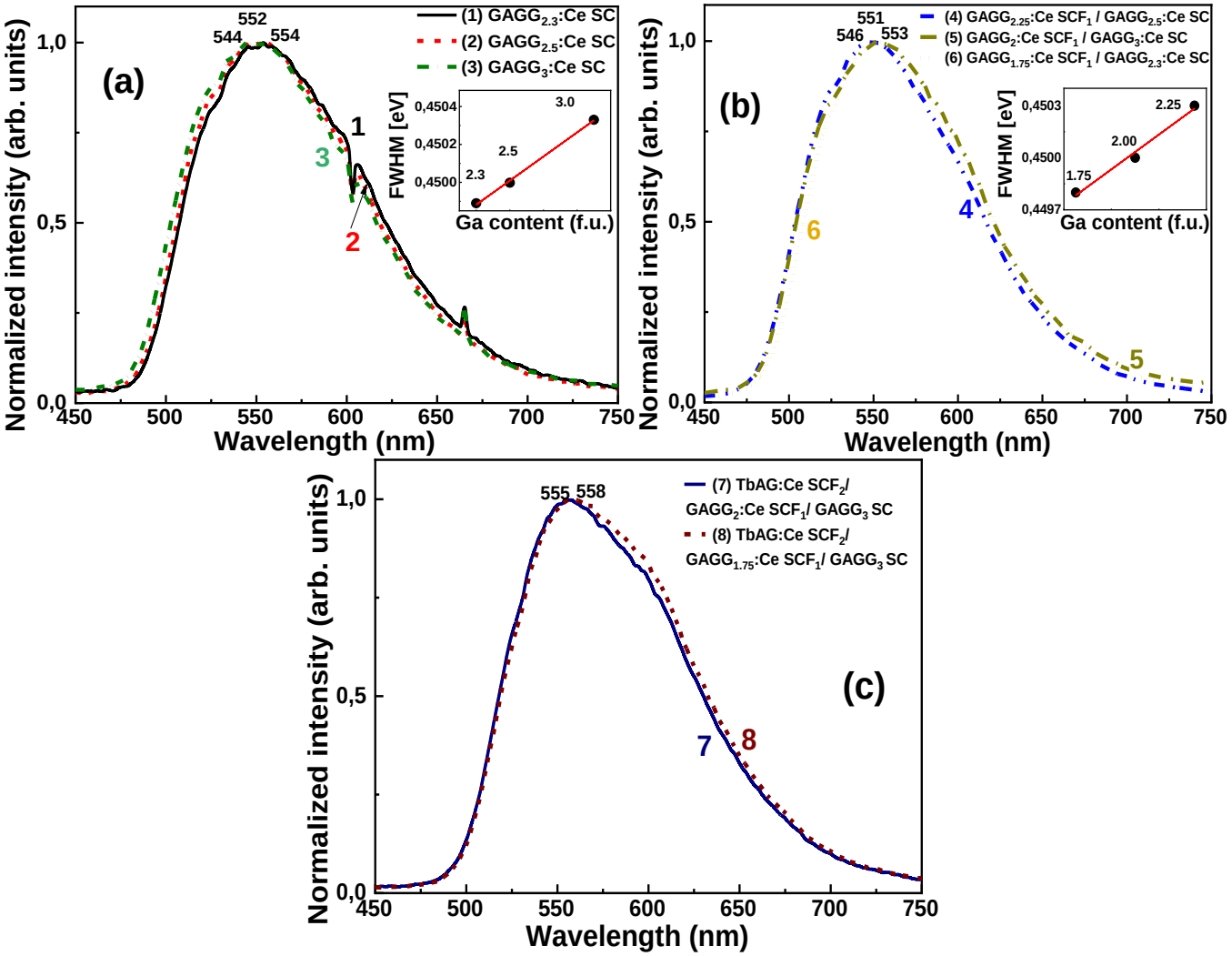

Fig. 4. RT normalized CL spectra of GAGG$_{2.3}$:Ce, GAGG$_{2.5}$:Ce and GAGG$_3$:Ce SC substrates (1-3, respectively) as well as two-layered GAGG$_{1.75-2.25}$ SCF$_1$/GAGG$_x$:Ce SCs (4-6) and TbAG:Ce SCF$_1$ / GAGG$_{1.75-2}$:Ce SCF$_1$ / GAGG$_3$:Ce SC (7, 8) epitaxial structures with different SCF thicknesses. The inserts shows the change of FWHM of Ce^{3+} emission bands in SC and SCF samples with increasing Ga content.

correspond to the $5d^1 \rightarrow 4f$ ($^2F_{5/2;7/2}$) transitions of Ce^{3+} ion in the respective garnet hosts. The peak positions of the Ce^{3+} luminescence bands in GAGG$_x$:Ce SCs are shifted into blue range of spectra and FWHM of these bands becomes a little bit wider with increasing the Ga content in the respective SCs samples (Fig. 4a, insert).

The CL spectra of the SCF parts of all $GAGG_{1.75\text{-}2.25}$ $SCF_1/GAGG_x$:Ce (x=2.3-3) SC composite scintillators consists also of the broad Ce^{3+} emission bands in the visible part of the spectra. The peak positions of the Ce^{3+} emission bands in $GAGG_x$:Ce SCF_1 were also shifted also into blue range of spectra and FWHM of these bands becomes larger with increasing the Ga content in the SCFs. As we mentioned above, the same effect is observed in the $GAGG_x$:Ce substrates on which these films were grown, and their spectra well overlap with the spectra of $GAGG_x$:Ce SCF_1 with the comparable concentration of Ga in the matrix. These trends can be explained by reduction/increase in the crystal field strength and electron-phonon interaction in the dodecahedral positions of the corresponding garnet hosts with different Ga/Al ratios [37].

The situation is quite different for the TbAG:Ce SCF_1 / $GAGG_{1.75\text{-}2}$:Ce SCF_1 / $GAGG_3$:Ce SC composite scintillator. A stronger shift of CL spectra of TbAG:Ce SCF_2 to 555-558 nm with respect to the $GAGG_3$:Ce substrate is observed due to increasing the crystal field strength in the dodecahedral position of garnet host in TbAG matrix. Small shift in the positions of Ce^{3+} bands TbAG:Ce SCFs with nominally the same content (Fig. 3c), can be explained by some deviation in the Ce^{3+} concentration in the mentioned samples and respective reabsorption of the Ce^{3+} luminescence in the films with different thicknesses [23]. This deviation may arise also because of slightly different conditions during the LPE growth of these samples onto $GAGG_x$:Ce SCs with varying concentrations of gallium.

Light yield and decay times of SCFs and composite scintillators. Under α-particle excitation from a ^{239}Pu (5.15 MeV) source, the scintillation LY and decay kinetics of the $GAGG_{1.75\text{-}2.25}$:Ce SCF_1/ $GAGG_x$:Ce SC; x=2.3-3 and TbAG:Ce $SCF_1/GAGG_{1.75\text{-}2}$:Ce $SCF_1/GAGG_3$:Ce SC composite scintillators with different SCF thicknesses were studied in comparison with $GAGG_{2.3}$:Ce, $GAGG_{2.5}$:Ce and $GAGG_3$:Ce SC substrates. The main obtained results were presented in Table 2.

Under the α–particles excitation, the LY of the $GAGG_x$:Ce SC substrates shows the notable dependence on the Ga concentration. Namely, with increasing the Ga content from 2.3 to 3.0, the LY decreases from 362% to 314 % compared to the reference sample. However, the change in the Ga concentration is also strongly reflected in the scintillation decay kinetics of the $GAGG_x$:Ce SC substrates.

Table 2. The LY and decay times $t_{1/e}$, $t_{1/10}$ and $t_{1/20}$ of the film and crystal parts of composite scintillators under α- particles excitation of ^{239}Pu (5.15 MeV) source, measuring with 12 μm shaping time gate in comparison with standard YAG:Ce SCF sample with a LY of 2 650 photons/MeV.

N	**Samples**	**LY, %**	**$t_{1/e}$, ns**	**$t_{1/10}$, ns**	**$t_{1/20}$, ns**
0	YAG:Ce SCF	100	-	-	-
1	$GAGG_3$:Ce	314	243	619	918

2	$GAGG_{2.5}$:Ce	340	298	704	982
3	$GAGG_{2.3}$:Ce	362	326	775	1097
4	$GAGG_2$:Ce SCF_1 / $GAGG_3$:Ce SC	52	108	233	330
5	$GAGG_{2.25}$:Ce SCF_1 / $GAGG_{2.5}$:Ce	21	86	180	267
6	$GAGG_{1.75}$:Ce SCF_1 / $GAGG_{2.3}$:Ce SC	67	113	235	314
7	TbAG:Ce SCF_2/ $GAGG_2$:Ce SCF_1/$GAGG_3$:Ce SC	120	157	1207	2041
8	TbAG:Ce SCF_2/ $GAGG_{1.75}$:Ce SCF_1/$GAGG_3$:Ce SC	135	411	1870	2693

Indeed, the increase of Ga content from x=2.3 to 3.0 leads to strong acceleration of the scintillation decay kinetics of the substrate samples (Table 1). Such changes in scintillation decay kinetics are very beneficial for creating composite scintillators because they provide additional scintillation decay profiles coming from the SC and SCF parts.

It is important to note here that in comparison with SC counterparts, the LY of $GAGG_x$:Ce SCF_1 is significantly lower (by 5-12 times) than that for their bulk SC counterparts (Table 1). This can be explained by the large negative influence of Pb^{2+} contaminant from the flux related dopant and formation of Ce^{4+}-Pb^{2+} pair centers during the samples growth using the LPE method [33-35]. It is noteworthy that the LY of garnet scintillators containing Ce^{4+} -A^{2+} (Ca^{2+}, Mg^{2+}, Pb^{2+}) pairs consistently demonstrates a lower intensity compared to the LY of Ce^{3+} doped garnets [33-35] and other oxides, as indicated in references [36, 37]. On the other hand, TbAG:Ce SCF_2/ $GAGG_{1.75-2}$:Ce SCF_1/$GAGG_3$:Ce SC composite scintillators exhibit higher LY in comparison with the reference YAG:Ce SCF sample. However, the LY of TbAG:Ce SCF_1 scintillators is also significantly (approximately by 3 times) lower than that for $GAGG_x$:Ce substrates. This observation can be also explained by the influence of lead dopant on the scintillation properties of TbAG:Ce SCF_2.

The varied decay patterns observed in the scintillation curves (Table 2) provide a fingerprint for differentiating $GAGG_x$:Ce and TbAG:Ce scintillators, particularly crucial when these materials are combined and penetrated with diverse types of radiation. In the following sections, we present the results of extended studies of scintillation pulse height spectra (PHS) and the decay kinetics of the studied epitaxial structures, which confirm this assumption.

Pulse height spectra (PHS). The PHS for composite scintillators based on the $GAGG_{1.75-2.25}$:Ce SCF_1 /$GAGG_x$:Ce SC; x=2.3-3 and TbAG:Ce SCF_1/$GAGG_{1.75-2}$:Ce SCF_1/$GAGG_{3:}$Ce SC epitaxial structures with different SCF thicknesses (Table 1) compared to the PHS of $GAGG_x$:Ce (x-2.3-3) SC substrates are demonstrated in Figs. 5(a-b) and 4(c-d), respectively. For excitation composite scintillators, ^{239}Pu and ^{137}Cs were used as sources of α-particles and γ-rays, respectively.

Each of the main peaks in Fig. 4a and 4c represents the complete absorption of α-particles in comparison with an energy of 5.15 MeV. The observation from Fig. 4(a – c) indicates a notably higher scintillation efficiency for all $GAGG_x$:Ce SC substrates as compared with the film parts of composite

scintillators. This can be explained by the above mentioned negative effects of Pb^{2+} flux-related dopants and the creation of Pb^{2+}-Ce^{4+} pairs that are responsible for the lower LY of SCF scintillators relatively to substrates with the quite close content (see Table 2).

It is worth noting that for both types of composite scintillators, the different positions of the main PHS peaks for SCF and substrates clearly show that the SCF parts completely absorb the α-particles of the

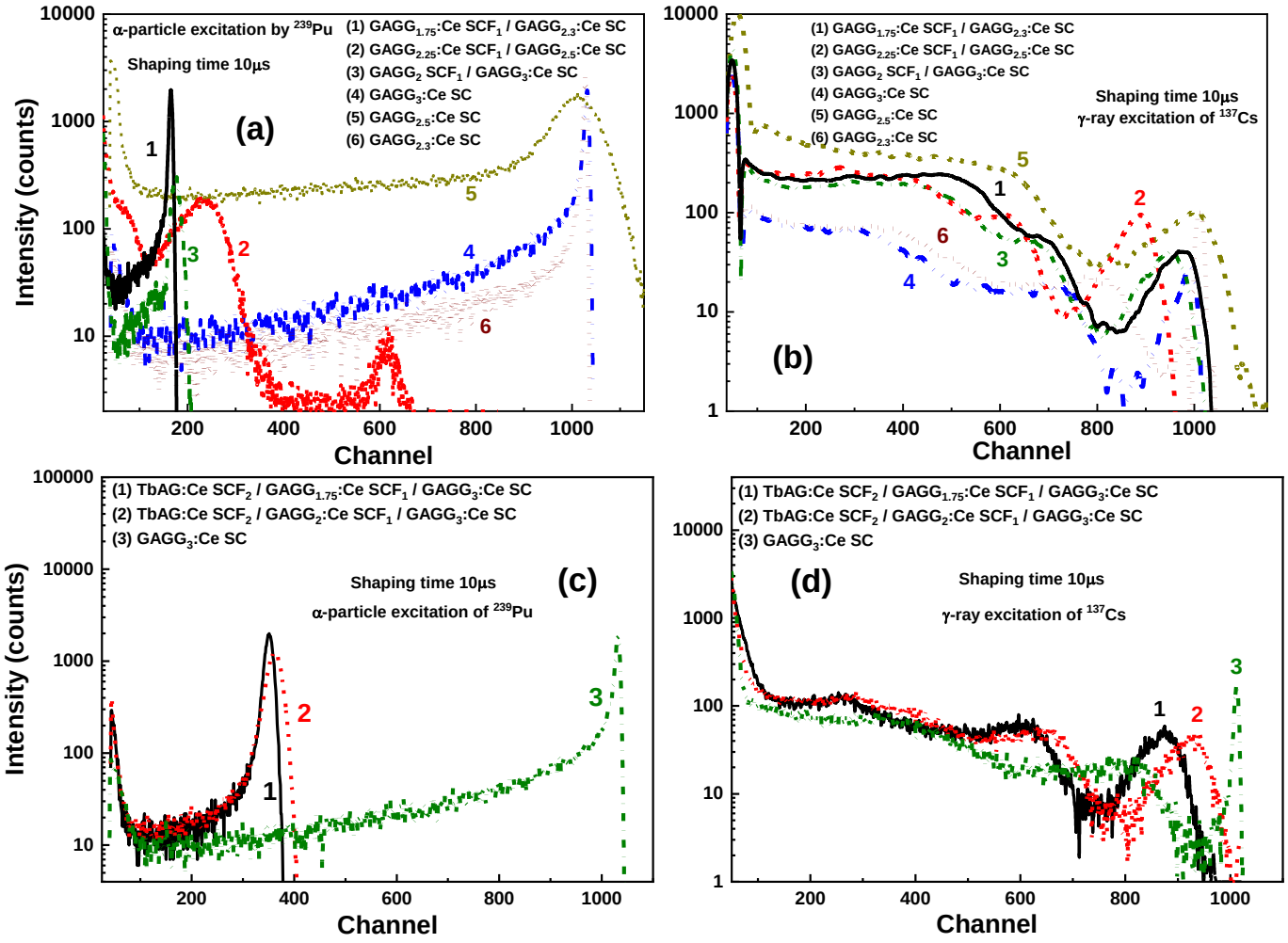

Fig. 5. PHS of composite scintillators based on the $GAGG_x$:Ce SCF_1 (x=1.75–2.25) / GAGG:Ce SC (x=2.3; 2.5 and 3) epitaxial structures (a, b) and TbAG:Ce SCF_2/$GAGG_x$:Ce SCF_1 (x=1.75–2.25) /$GAGG_3$:Ce SC epitaxial structures (c, d) with different SCF thicknesses compared to PHS of $GAGG_x$:Ce substrates measured with 10 μs shaping time under α-particle excitation from ^{239}Pu (5.15 MeV) source (Fig. 4a, c) and γ-quantum excitation from ^{137}Cs (662 keV) source (Fig. 4b, d).

^{239}Pu source (Fig. 5a and 5c). However, for $GAGG_{2.25}$:Ce SCF_1 /$GAGG_{2.5}$:Ce SC sample (Fig. 5a, curve 2), the main band is much wider and shifted in the direction of increasing channels more significantly than

others analogues for the same sample set. The broad low-intensity peak in the range, where $GAGG_x$:Ce SC has main peaks, indicates that α-particles of ^{239}Pu source partly penetrate through SCF of the composite scintillator and excite the substrate. Most likely it is possible because of thickness of the film (15 μm), which is relatively smaller than that in another SCFs from the set of similar samples.

Under γ-ray excitation from ^{137}Cs source of $GAGG_x$:Ce SCF_1 (x=1.75–2.25)/$GAGG_x$:Ce SC (x=2.3; 2.5, 3) and TbAG:Ce SCF_2/$GAGG_x$:Ce SCF (x=1.75–2.25)/$GAGG_3$:Ce SC composite scintillators, the main PHS peaks correspond to the full absorption of γ-quantum radiation with an energy of 662 keV (Fig. 4b and 4d, respectively). The low-energy line of a ^{137}Cs source corresponds to the additional peak at 32 keV. The main peaks for both sets of composite scintillators in Fig. 5b and 5d are located in close positions for the first type of composite scintillators and respective $GAGG_x$:Ce SC substrate. This means that γ-rays excite mainly the substrate scintillators in $GAGG_x$:Ce SCF_1/$GAGG_x$:Ce and TbAG:Ce SCF_2/$GAGG_{1.75}$:Ce SCF_1/$GAGG_3$:Ce SC epitaxial structures, and the influence of SCF scintillators on the total LY (Table 1) of this composite scintillator is insignificant. Meanwhile, for the TbAG:Ce SCF_2 (15 μm)/$GAGG_2$:Ce SCF_1 (105 μm)/ $GAGG_3$:Ce SC composite scintillator the position of main peak under γ-ray excitation is notably shifted with respect the position of respective another sample with the SCF_1/SCF_2 thickness of 29 μm/38 μm and $GAGG_3$:Ce substrate due to considerable absorption of γ-quanta by thicker (105 μm) SCF_1 sample and lower LY of this film scintillator in comparison with the LY of substrate (Table 1, Fig. 5d, curve 1).

Scintillation decay kinetics. Analysis of the differences in scintillation decay curves of epitaxial structures doped with Ce^{3+} after excitation by α-, β-particles, and γ-quanta is a key point in the creation of composite scintillators. In this work, this analysis was performed on samples of the $GAGG_x$:Ce SCF_1 (x= 1.75–2.25)/GAGG:Ce SC (x=2.3-3) and TbAG:Ce SCF_2/$GAGG_x$:Ce SCF_1 (x=1.75–2)/$GAGG_3$:Ce SC composite scintillators with different SCF thicknesses (Fig.6 (a–c) and 6 (d, e), respectively).

As a quantitative measure of the separation between two scintillation signals, figure-of-merit (FOM) (Eq. 1) values were used to calculate the difference in scintillation decay times under simultaneous registration of the α-, β-, and γ-excitations:

$$\boldsymbol{FOM_{\beta\gamma}} = \left|\frac{(t_\beta - t_\gamma)}{(t_\beta + t_\gamma)}\right| \quad \boldsymbol{FOM_{\alpha\beta}} = \left|\frac{(t_\alpha - t_\beta)}{(t_\alpha + t_\beta)}\right|; \quad \boldsymbol{FOM_{\alpha\gamma}} = \left|\frac{(t_\alpha - t_\gamma)}{(t_\alpha + t_\gamma)}\right|; \qquad (1).$$

In general, for effective separation of the two decay curves, the corresponding decay times at the selected decay intensity level must differ by at least 1.5 times. This means that the corresponding FOM values must be at least 0.2 or larger.

It is seen in Fig. 6 that the scintillation decay kinetics of substrates under the selected type of excitation is essentially dependent on the Al/Ga ratio in the appropriate garnet compounds due to the specific

interactions of these types of radiation with the materials. To be more precise, the scintillation decay kinetics of $GAGG_x$:Ce SC substrates under β-particle and γ-ray excitations becomes notable faster with increasing Ga content (Fig. 6 a-c, curve 2, 3) using the same excitation source. This give additional ability for separation of the decay profiles from the film and substrate parts of composite scintillators. However, the separation between the decay profiles under β-particle and γ-ray excitations is weak for all samples of $GAGG_x$:Ce SCF_1/$GAGG_x$Ce SC composite scintillators (Fig. 6 a, b). These type of composite scintillators show also

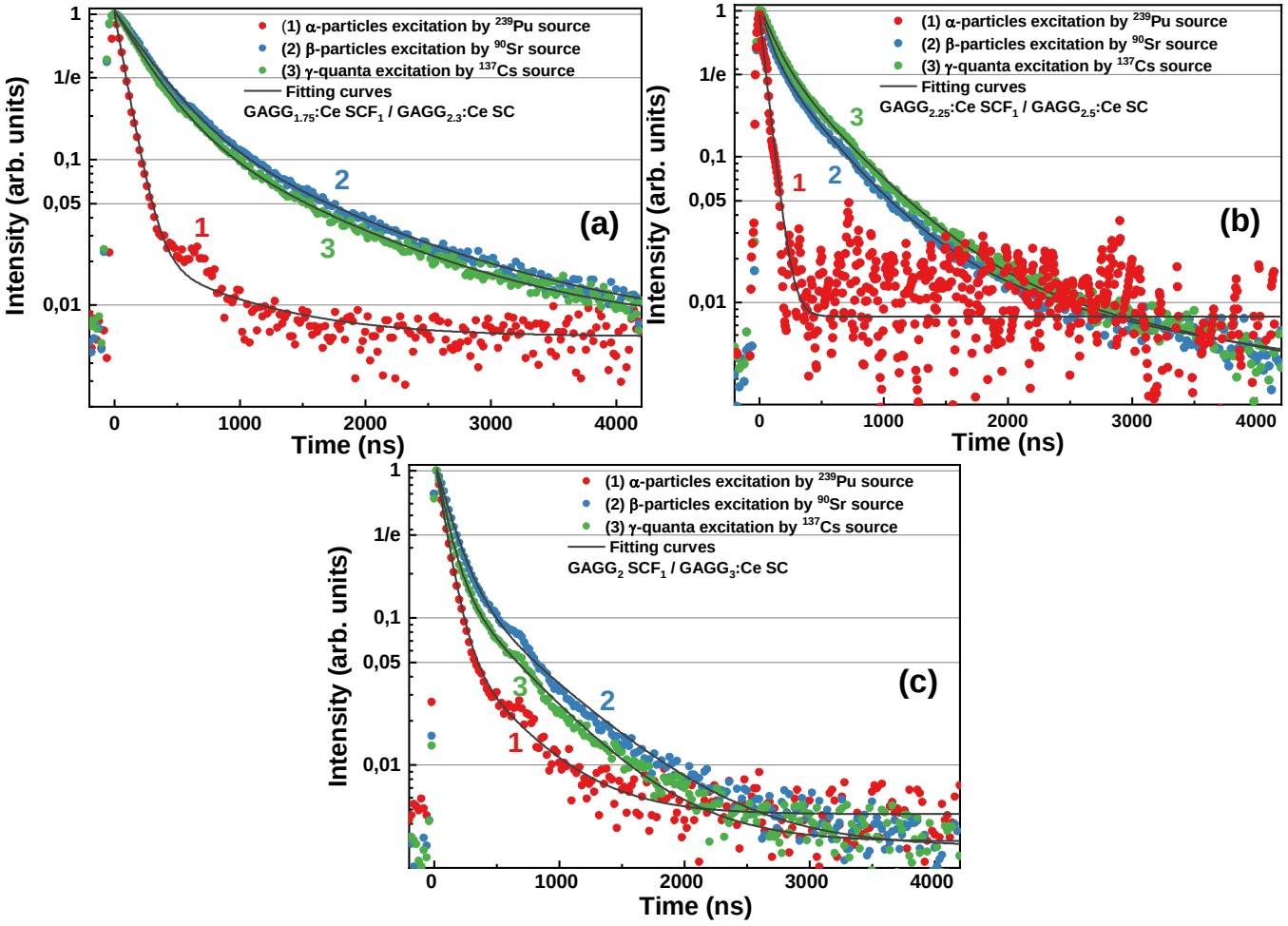

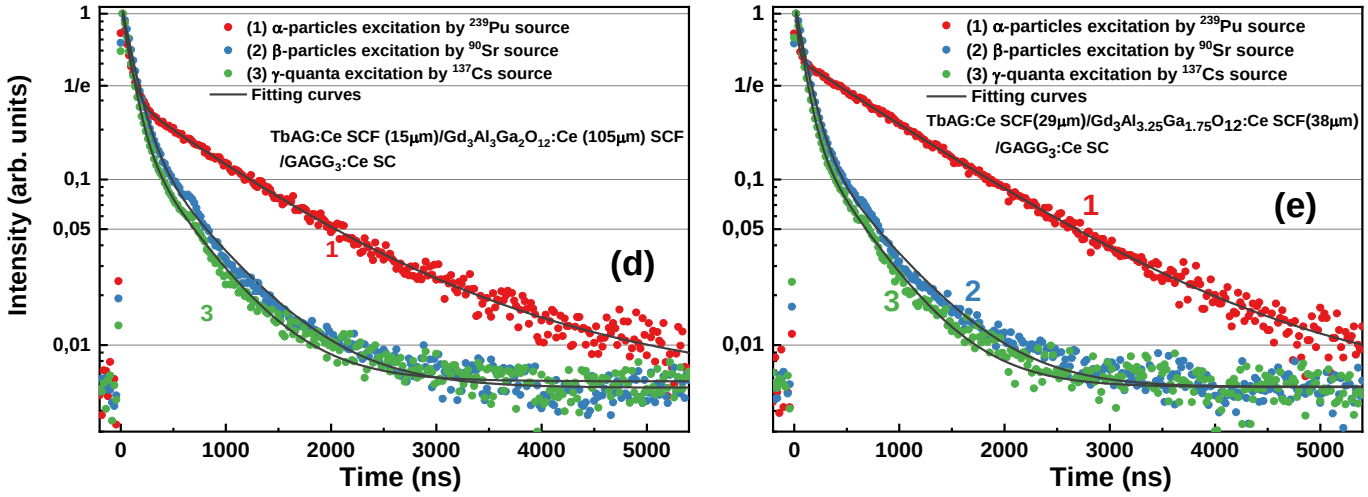

Fig. 6. Scintillation decay kinetics of composite scintillators based on the $GAGG_{1.75\text{-}2.25}$:Ce $SCF_1/GAGG_x$:Ce (x=2.3, 2.5 and 3) SC epitaxial structures with different SCF thickness (a-c) and TbAG:Ce $SCF_2/GAGG_{1.75\text{-}2}$:Ce $SCF_1/GAGG_3$:Ce SCs (d, e) epitaxial structures with different thickness of the TbAG:Ce SCF scintillators under excitation by α-, β- particles and γ–quanta.

significantly faster scintillation decay in the initial stage in the case of α-particle excitation in comparison with β-particle and γ-ray excitations (Fig. 6 a-c).

On the other hand, the scintillation decay time in the SCFs scintillators under α-particles excitation can also be effectively controlled by changing the concentration of Ga and Al in the mixed $GAGG_x$:Ce garnets. This is confirmed by the acceleration of the decay kinetics with the increase in the Ga concentration in the SCF sample with x=2.25 (Fig.6b, curve 1) compared to the scintillation decay of SCFs with Ga x=1.75 and 2 content (Fig. 6a and 6c, curves 1). The large difference in the scintillation decay kinetics of SCF scintillators, grown from PbO-based fluxes, compared to the substrates is also caused by the formation of Pb^{2+}–Ce^{4+} centers in them, which strongly accelerates the scintillation decay of the films (Fig. 6, a-c). However, it is necessary to take into account that contamination with Pb^{2+} ions from the $PbO\text{-}B_2O_3$ flux combined with a high Ga content also significantly reduces the LY of the SCF layers (Fig. 6b).

As a result of a larger FOM ratios (Fig. 7a and Tab. 3), calculated after excitations by different types of ionizing radiation, the $GAGG_{1.75\text{-}2.25}$:Ce $SCF_1/GAGG_x$:Ce SCs composite scintillator look more promising for following optimization figure of merit in comparing with third composition of two-layered composite scintillators. Indeed, the epitaxial structures grown onto $GAGG_{2.3}$:Ce and $GAGG_{2.5}$:Ce SC substrates has significantly better characteristics (FOM values) under the excitation of different sources (Fig.7a, curves 4-6 and Tab. 3) in comparison with composite scintillators based on $GAGG_3$:Ce SC

substrate (Fig.7, curves 7-9 and Tab. 3).

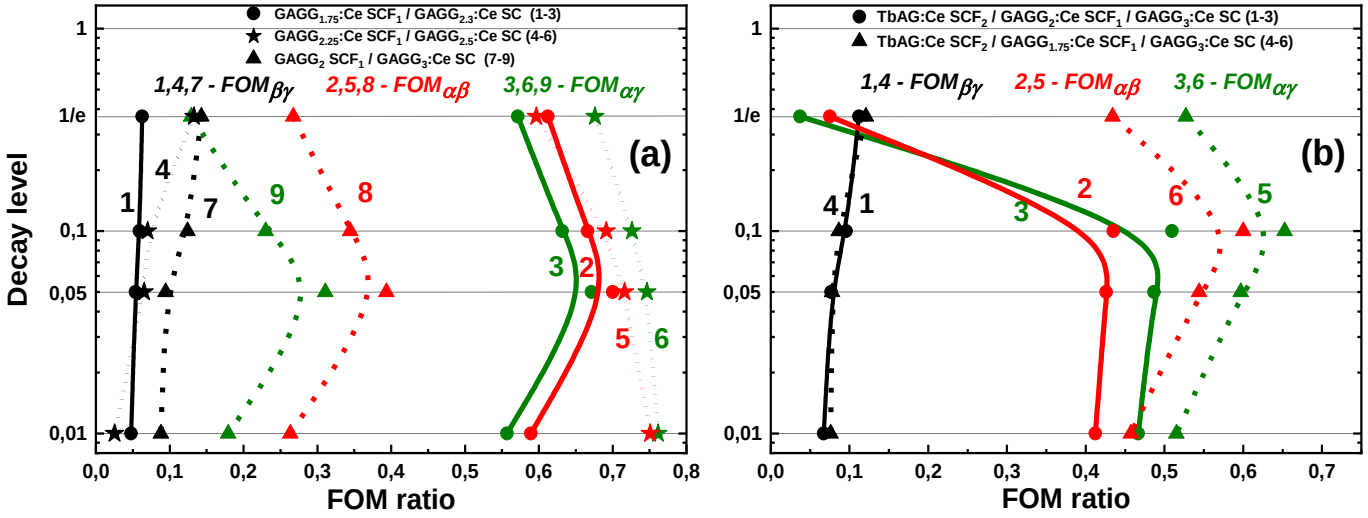

Fig. 7. FOM values for $GAGG_{1.75\text{-}2.25}$:Ce SCF_1 / $GAGG_x$:Ce SC (x=2.3, 2.5, 3) (a) and TbAG:Ce SCF_2 / $GAGG_{1.75\text{-}2}$:Ce SCF / $GAGG_3$:Ce SC (b) composite scintillators with different TbAG:Ce SCF_2 thickness under simultaneous β/γ (back), α/β (red) and α/γ (green) excitations.

Table 3. Comparison of the difference in the best FOM values under β/γ, α/β and α/γ excitations for all sample of composite scintillators. The bracket indicate the registration level of scintillation decay.

N	Sample	$FOM_{\beta\gamma}$	$FOM_{\alpha\beta}$	$FOM_{\alpha\gamma}$
1	$GAGG_2$:Ce SCF_1 / $GAGG_3$:Ce SC	0.14 (1/e)	0.39 (0.05)	0.31 (0.05)
2	$GAGG_{2.25}$:Ce SCF_1 / $GAGG_{2.5}$:Ce	0.05 (1/e)	0.75 (0.01)	0.76 (0.01)
3	$GAGG_{1.75}$:Ce SCF_1 / $GAGG_{2.3}$:Ce SC	0.06 (1/e)	0.70 (0.05)	0.67 (0.05)
4	TbAG:Ce SCF_2/ $GAGG_2$:Ce SCF_1/$GAGG_3$:Ce SC	0.11 (1/e)	0.43 (0.1)	0.48 (0.1)
5	TbAG:Ce SCF_2/ $GAGG_{1.75}$:Ce SCF_1/$GAGG_3$:Ce SC	0.12 (1/e)	0.60 (0.1)	0.65 (0.1)

The next step in this study was the growth and investigation of three-layered TbAG:Ce SCF_2/ $GAGG_{1.75\text{-}2}$:Ce SCF_1/$GAGG_3$:Ce SC (b) composite scintillators. Since the scintillation decay time of TbAG:Ce SCF_2 scintillator is much longer relative to the $GAGG_x$:Ce SC substrate, it was decided to use a faster scintillator from the set in order to obtain a greater separation of signals originating from different parts of the composite scintillator. The solution of this task was to use the two-layered $GAGG_{1.75}$:Ce SCF_1/ $GAGG_3$:Ce SC composite scintillator that showed the fastest decay kinetics under β- and γ- excitations and large β/γ decay time separation, with the additional top-layer in the form of TbAG:Ce SCF_2 with relatively slow scintillation decay. Indeed, as can be seen from Fig.6 (c–d), there is a significant difference of the scintillation curves in both TbAG:Ce SCF_1/$GAGG_{1.75\text{-}2}$:Ce SCF_2/ $GAGG_3$:Ce samples, which differ

in the thickness of the upper (15 and 29 μm) and the middle (105 and 38 μm) films as well as Ga content in them (x=2 and 1.75), respectively. As can be seen from (Fig.5 d, e), the shape of the decay curves (1), corresponding to excitation by ^{239}Pu source, indicates that α-particles are fully absorbed in the TbAG:Ce SCF parts of composite scintillators. Such a more complex, multicomponent scintillation decay kinetics is typical for Ce^{3+} doped Tb^{3+}-based garnet matrices, where energy transfer through the sublattice of Tb^{3+} cations is more significant [38, 39] in comparison with $GAGG_x$:Ce garnets. Such a significant difference in the curves shows that it is possible to effectively separate the signals originating from α- and β-particles and γ-quanta based on the calculated FOM values for composite scintillators TbAG:Ce SCF_2 / $GAGGG_2$:Ce SCF_1/$GAGG_3$:Ce SC and TbAG:Ce SCF_2 / $GAGG_{1.75}$:Ce SCF_1 /$GAGG_3$:Ce SC sample (Fig. 7b and Tab. 3). According to these data, the best scintillation figure of merit for simultaneous registering the mixed α/β and α/γ fluxes was obtained for the TbAG:Ce SCF_2 / $GAGG_{1.75}$:Ce SCF_1 /$GAGG_3$:Ce SC sample at 10% (0.1 level) of scintillation decay (Fig. 7b and Table 3). From other hand, the sample with large $Gd_3Al_3Ga_2O_{12}$:Ce SCF_1 thickness possess little bit larger $FOM_{\beta\gamma}$ value.

Comparing these values, it can be seen that $FOM_{\alpha\gamma}$ and $FOM_{\alpha\beta}$ for composite scintillators under study are large enough to provide effective separate portions of the α/γ and α/β excitations. However, the obtained highest value of $FOM_{\beta/\gamma}$=0.11-0.12 is not satisfactory for effective separation of β/γ excitations and requires an improvement to at least a value of 0.2. The first way for improvement $FOM_{\beta/\gamma}$ ratio can be connected with increasing thickness of the SCF_1 layer, intended mainly for the absorption of β-particles, at least to 100 μm. Meanwhile, as can be seen from Figs. 6 and 7, increasing $Gd_3Al_3Ga_2O_{12}$:Ce SCF thickness from 38 μm to more than 100 μm does not significantly improve the properties of this type of three-layer composite scintillator for β/γ separation. Another method for improvement $FOM_{\beta/\gamma}$ value can be conected with increasing substrate thickness at least to 1 mm. In this way, the contribution of $GAGG_3$:Ce SC substrate scintillators in the registration of γ-quanta will be higher and the β/γ excitation separation may probably be larger.

4. Conclusions

The prototypes of new two-layered and three-layered composite scintillators for simultaneous registration of the various components of mixed ionization radiation fluxes on the basis of $GAGG_x$:Ce (x=1.75-2.25) and TbAG:Ce single crystalline films (SCFs) as well as $GAGG_x$:Ce (x=2.3-3.0) single crystal (SC) substrates have been created using the LPE growth method from the melt-solutions based on $PbO-B_2O_3$ flux. Absorption, cathodoluminescence, pulse height spectra, light yield (LY), and scintillation decay kinetics under excitation by α– (^{239}Pu) and β- (^{90}Sr) particles as well as γ–quanta (^{137}Cs) were

measured to characterize the luminescent and scintillation properties of the film and bulk crystal parts of such composite scintillators.

It has been found that influence of Pb^{2+} impurity introduced from the flux and the formation of Pb^{2+} – Ce^{4+} pair centers give rise to significantly (by several times) lower LY of $GAGG_x$:Ce and TbAG:Ce SCF parts of composite scintillators under α-particle excitation by ^{239}Pu source in comparison with all of $GAGG_x$:Ce SC substrates. However, the scintillation response of $GAGG_x$:Ce SCFs is significantly faster than that of their $GAGG_x$:Ce SC counterparts. This gives additional possibility for separation of the signals coming from the film and bulk parts of composite film(s)-crystal scintillators even in the case close SCF and substrate compositions.

Additionally, $GAGG_x$:Ce (x=1.75-2.25) and TbAG:Ce SCFs scintillators under α-particle excitation have different scintillation decay profiles compared to the mentioned bulk crystal substrates, due to the differences in the Ga content and structure of the emission centers (Ce^{3+} in the substrates and both Ce^{3+} and Pb^{2+}–Ce^{4+} centers in SCFs), as well as through the specific energy transfer mechanism to the Ce^{3+} ions in Tb^{3+}-based garnet matrices. As a result of the above mentioned properties of the films and substrate-scintillators, we have observed significant differences in the scintillation decay of the two-layered $GAGG_{1.75}$:Ce SCF_1/$GAGG_{2.3\text{-}2.5}$:Ce SC and three-layered TbAG:Ce SCF_2/$GAGG_{1.75\text{-}2}$:Ce SCF_1/$GAGG_3$:Ce composite scintillators under α- and β-particles and γ-ray excitations due to the dominant absorption of α-particles by the corresponding upper SCF scintillators and β-particles and γ-rays partly in the first and second SCF layers and mainly by substrate-scintillators.

Among the two types of composite scintillators studied in this work, the $GAGG_x$:Ce SCF (x=1.75, 2.25)/ $GAGG_{2.3\text{-}2.5}$:Ce SC and TbAG:Ce SCF/$GAGG_{1.75\text{-}2}$:Ce SCF/$GAGG_3$:Ce CS epitaxial structures possess the scintillation properties suitable for effective registration of the different kinds of ionization radiation, especially for simultaneous detection α/β mixed radiation with respective $FOM_{\alpha\beta}$ =0.39-0.70 and 0.51-0.65 values and mixed α/γ radiation with $FOM_{\alpha\gamma}$=0.31-0.67 and 0.335-0.60 ratios, correspondingly. However, the highest $FOM_{\beta/\gamma}$=0.11-0.12 values for the mentioned scintillators are not satisfactory for the effective separation of mixed β/γ excitation and requires improvement to at least a value of 0.2 by means of increasing the thickness of $GAGG_{1.75\text{-}2}$:Ce SCF scintillators at least to 100 μm and $GAGG_x$:Ce substrate thickness above 1 mm for both types of developed composite scintillators. It should be also noted that the most effective method of simultaneous recording the mixed ionizing radiation is to record it at a level of 5–10% of the peak scintillation decay intensity.

The results obtained in this work provide an understanding of the potential use of these type composite

scintillators in the creation of multilayer "all solid state" scintillation detectors for analysis of different mixed radiation fluxes including radiation monitoring and medical applications.

Acknowledgement. The work was performed in the frameworks of Polish National Centre (NCN) OPUS 24 LAP No 2022/47/I/ST8/02600 project.

References

[1] Yu.V. Zorenko, S.S. Novosad, M.V. Pashkovskii, A.B. Lyskovich, V.G. Savitskii, M.M. Batenchuk, P.S. Malyutenkov, N.I. Patsagan, I.V. Nazar, V.I. Gorbenko, Epitaxial structures of garnets as scintillation detectors of ionizing radiation, J Appl Spectrosc. 52 (1990) 645–649. https://doi.org/10.1007/bf00662203.

[2] P. Dorenbos, C. van Eijk, E. Van Loef, M. Globus, B. Grinyov, M. Ratner, V. Tarasov, Yu.Zorenko. Heavy Oxide Scintillators: Bulk Crystals and Thin Films for radiation Monitoring of Environment and Biologial Objects, Moscow, Faculty of Physics, M.V.Lomonosov Moscow State University, 2000, P. 577-582.

[3] M. Globus, B. Grinyov, M. Ratner, V. Tarasov, V. Lyubinskiy, Yu. Vydai, A. Ananenko, Yu. Zorenko, V. Gorbenko, I. Konstankevych, New type of scintillation detectors for biological, medical, and radiation monitoring applications, IEEE Trans. Nucl. Sci. 51 (2004) 1297–1303. https://doi.org/10.1109/tns.2004.830113.

[4] Y. Zorenko, V. Gorbenko, T. Voznyak, I. Konstankevych, V. Savchyn, M. Batentschuk, A. Winnacker, C.J. Brabec, Scintillators Based on $CdWO_4$ and $CdWO_4$:Bi Single Crystalline Films, IEEE Trans. Nucl. Sci. 59 (2012) 2281–2285. https://doi.org/10.1109/tns.2012.2201171.

[5] S. Kurosawa, A. Yoshikawa, V. Gorbenko, T. Zorenko, S. Witkiewicz-Lukaszek, A. Fedorov, Yu. Zorenko, Composite Scintillators Based on the Films and Crystals of $(Lu,Gd,La)_2Si_2O_7$ Pyrosilicates, IEEE Trans. Nucl. Sci. 67 (2020) 994–998. https://doi.org/10.1109/tns.2020.2983657.

[6] J.A. Mares, V. Gorbenko, R. Kucerkova, P. Prusa, A. Beitlerova, T. Zorenko, M. Pokorny, S. Witkiewicz-Łukaszek, Y. Syrotych, C. D'Ambrosio, M. Nikl, O. Sidletskiy, Y. Zorenko, Scintillation Characteristics of the Single-Crystalline Film and Composite Film-Crystal Scintillators Based on the Ce^{3+}-Doped $(Lu,Gd)_3(Ga,Al)_5O_{12}$ Mixed Garnets under Alpha and Beta Particles, and Gamma Ray Excitations, Materials. 15 (2022) 7925. https://doi.org/10.3390/ma15227925.

[7] M. Nikl, Nanocomposite, Ceramic, and Thin Film Scintillators, 1st Edition, Jenny Stanford, 2016.

[8] S. Witkiewicz-Lukaszek, V. Gorbenko, T. Zorenko, K. Paprocki, O. Sidletskiy, A. Fedorov, R. Kucerkova, J.A. Mares, M. Nikl, Y. Zorenko, Epitaxial growth of composite scintillators based on $Tb_3Al_5O_{12}$: Ce single crystalline films and $Gd_3Al_{2.5}Ga_{2.5}O_{12}$:Ce crystal substrates, CrystEngComm. 20 (2018) 3994–4002. https://doi.org/10.1039/c8ce00536b.

[9] S. Witkiewicz-Lukaszek, V. Gorbenko, T. Zorenko, O. Sidletskiy, I. Gerasymov, A. Fedorov, A. Yoshikawa, J.A. Mares, M. Nikl, Y. Zorenko, Development of composite scintillators based on single crystalline films and crystals of Ce^{3+}-doped $(Lu,Gd)_3(Al,Ga)_5O_{12}$ mixed garnet compounds, Cryst. Growth Des. 18 (2018) 1834–1842. https://doi.org/10.1021/acs.cgd.7b01695.

[10] S. Witkiewicz-Lukaszek, V. Gorbenko, T. Zorenko, Y. Syrotych, J.A. Mares, M. Nikl, O. Sidletskiy, P. Bilski, A. Yoshikawa, Y. Zorenko, Composite detectors based on single-crystalline films and single crystals of garnet compounds, Materials (Basel). 15 (2022) 1249. https://doi.org/10.3390/ma15031249.

[11] A. Koch, C. Raven, P. Spanne, A. Snigirev, X-ray imaging with submicrometer resolution employing transparent luminescent screens, J. Opt. Soc. Am. A Opt. Image Sci. Vis. 15 (1998) 1940. https://doi.org/10.1364/josaa.15.001940.

[12] T. Martin, A. Koch, Recent developments in X-ray imaging with micrometer spatial resolution, J. Synchrotron Radiat. 13 (2006) 180–194. https://doi.org/10.1107/s0909049506000550.

[13] S. Witkiewicz-Lukaszek, A. Mrozik, V. Gorbenko, T. Zorenko, P. Bilski, A. Fedorov, Y. Zorenko, LPE Growth of Composite Thermoluminescent Detectors Based on the $Lu_{3-x}Gd_xAl_5O_{12}$:Ce Single Crystalline Films and YAG:Ce Crystals, Crystals. 10 (2020) 189. https://doi.org/10.3390/cryst10030189.

[14] S. Witkiewicz-Lukaszek, V. Gorbenko, T. Zorenko, Y. Zorenko, W. Gieszczyk, A. Mrozik, P. Bilski, Composite thermoluminescent detectors based on the Ce^{3+} doped LuAG/YAG and YAG/LuAG epitaxial structures, Radiation Measurements. 128 (2019) 106124. https://doi.org/10.1016/j.radmeas.2019.106124.

[15] S. Witkiewicz-Lukaszek, A. Mrozik, V. Gorbenko, T. Zorenko, P. Bilski, Y. Syrotych, Y. Zorenko, Development of the Composite Thermoluminescent Detectors Based on the Single Crystalline Films and Crystals of Perovskite Compounds, Materials. 15 (2022) 8481. https://doi.org/10.3390/ma15238481.

[16] A. Mrozik, P. Bilski, W. Gieszczyk, M. Kłosowski, S. Witkiewicz-Łukaszek, V. Gorbenko, T. Zorenko, Y. Zorenko, Application of the LPE-Grown LuAG: Ce Film/YAG Crystal Composite Thermoluminescence Detector for Distinguishing the Components of the Mixed Radiation Field, Materials. 15 (2022) 8708. https://doi.org/10.3390/ma15248708.

[17] P. Prusa, M. Kucera, J.A. Mares, Z. Onderisinova, M. Hanus, V. Babin, A. Beitlerova, M. Nikl, Composition tailoring in Ce-doped multicomponent garnet epitaxial film scintillators, Cryst. Growth Des. 15 (2015) 3715–3723. https://doi.org/10.1021/acs.cgd.5b00309.

[18] M. Klimczak, M. Malinowski, J. Sarnecki, R. Piramidowicz, Luminescence properties in the visible of Dy:YAG/YAG planar waveguides, J. Lumin. 129 (2009) 1869–1873. https://doi.org/10.1016/j.jlumin.2009.04.073.

[19] J. Iwanowska, L. Swiderski, T. Szczesniak, P. Sibczynski, M. Moszynski, M. Grodzicka, K. Kamada, K. Tsutsumi, Y. Usuki, T. Yanagida, A. Yoshikawa, Performance of cerium-doped $Gd_3Al_2Ga_3O_{12}$ (GAGG:Ce) scintillator in gamma-ray spectrometry, Nucl. Instrum. Methods Phys. Res. A. 712 (2013) 34–40. https://doi.org/10.1016/j.nima.2013.01.064.

[20] N.J. Cherepy, S.A. Payne, B.W. Sturm, S.P. O'Neal, Z.M. Seeley, O.B. Drury, L.K. Haselhorst, B.L. Rupert, R.D. Sanner, P.A. Thelin, S.E. Fisher, R. Hawrami, K.S. Shah, A. Burger, J.O. Ramey, L.A. Boatner, Performance of europium-doped strontium iodide, transparent ceramics and bismuth-loaded polymer scintillators, in: L.A. Franks, R.B. James, A. Burger (Eds.), SPIE Proceedings, SPIE, 2011.

[21] K. Kamada, T. Yanagida, J. Pejchal, M. Nikl, T. Endo, K. Tsutsumi, Y. Fujimoto, A. Fukabori, A. Yoshikawa, Crystal growth and scintillation properties of Ce doped $Gd_3(Ga,Al)_5O_{12}$ single crystals, IEEE Trans. Nucl. Sci. 59 (2012) 2112–2115. https://doi.org/10.1109/tns.2012.2197024.

[22] M. Nikl, A. Yoshikawa, Recent R&D trends in inorganic single-crystal scintillator materials for radiation detection, Adv. Opt. Mater. 3 (2015) 463–481. https://doi.org/10.1002/adom.201400571.

[23] Y. Zorenko, P.-A. Douissard, T. Martin, F. Riva, V. Gorbenko, T. Zorenko, K. Paprocki, A. Iskalieva, S. Witkiewicz, A. Fedorov, P. Bilski, A. Twardak, Scintillating screens based on the LPE grown $Tb_3Al_5O_{12}$:Ce single crystalline films, Opt. Mater. (Amst.). 65 (2017) 73–81. https://doi.org/10.1016/j.optmat.2016.09.066.

[24] Y. Syrotych, S. Witkiewich-Lukaszek, V. Gorbenko, T. Zorenko, R. Kucerkova, J.A. Mares, M. Nikl, O. Sidletskiy, K. Kamada, A. Yoshikawa, Y. Zorenko, New types of composite scintillators based on the single crystalline films and crystals of $Gd_3Al_{5-x}Ga_xO_{12}$:Ce garnets, Optical Materials: X. 17 (2023) 100227. https://doi.org/10.1016/j.omx.2023.100227.

[25] S. Witkiewicz-Lukaszek, V. Gorbenko, T. Zorenko, Y. Syrotych, R. Kucerkova, J.A. Mares, M. Nikl, O. Sidletskiy, A. Fedorov, S. Kurosawa, K. Kamada, A. Yoshikawa, Y. Zorenko, New types of composite scintillators based on the single crystalline films and crystals of $Gd_3(Al,Ga)_5O_{12}$:Ce mixed garnets, Mater. Sci. Eng. B Solid State Mater. Adv. Technol. 264 (2021) 114909. https://doi.org/10.1016/j.mseb.2020.114909.

[26] A. Dabkowski, M. Berkowski, G. Jasiołek, Czochralski crystal growth and aluminum segregation coefficient in yttrium gallium aluminum garnet, J. Cryst. Growth. 71 (1985) 371–376. https://doi.org/10.1016/0022-0248(85)90093-4.

[27] A. Yoshikawa, V. Chani, M. Nikl, Czochralski growth and properties of scintillating crystals, Acta Phys. Pol. A. 124 (2013) 250–264. https://doi.org/10.12693/aphyspola.124.250.

[28] K. Kamada, T. Endo, K. Tsutumi, T. Yanagida, Y. Fujimoto, A. Fukabori, A. Yoshikawa, J. Pejchal, M. Nikl, Composition engineering in cerium-doped $(Lu,Gd)_3(Ga,Al)_5O_{12}$ single-crystal scintillators, Cryst. Growth Des. 11 (2011) 4484–4490. https://doi.org/10.1021/cg200694a.

[29] J.B. Gruber, M.E. Hills, C.A. Morrison, G.A. Turner, M.R. Kokta, Absorption spectra and energy levels of Gd^{3+}, Nd^{3+}, and Cr^{3+} in the garnet $Gd_3Sc_2Ga_3O_{12}$, Phys. Rev. B Condens. Matter. 37 (1988) 8564–8574. https://doi.org/10.1103/physrevb.37.8564.

[30] D. Nakauchi, Y. Yoshida, N. Kawaguchi, T. Yanagida, Characterization of Ce-doped $RE_3Al_5O_{12}$ (RE=Tb, Dy, Ho, Er, Tm and Yb) single crystalline scintillators, J. Mater. Sci.: Mater. Electron. 30 (2019) 14085–14090. https://doi.org/10.1007/s10854-019-01774-3.

[31] P.A. Tanner, L. Fu, L. Ning, B.-M. Cheng, M.G. Brik, Soft synthesis and vacuum ultraviolet spectra of YAG:Ce^{3+} nanocrystals: reassignment of Ce^{3+} energy levels, J. Phys. Condens. Matter. 19 (2007) 216213. https://doi.org/10.1088/0953-8984/19/21/216213.

[32] Z. Xia, A. Meijerink, Ce^{3+}-Doped garnet phosphors: composition modification, luminescence properties and applications, Chem. Soc. Rev. 46 (2017) 275–299. https://doi.org/10.1039/c6cs00551a.

[33] S. Blahuta, A. Bessiere, B. Viana, P. Dorenbos, V. Ouspenski, Evidence and consequences of Ce^{4+} in LYSO:Ce, Ca and LYSO:Ce, Mg single crystals for medical imaging applications, IEEE Trans. Nucl. Sci. 60 (2013) 3134–3141. https://doi.org/hppt://dx.doi.org/10.1109/TNS.2013.2269700.

[34] M. Nikl, K. Kamada, V. Babin, J. Pejchal, K. Pilarova, E. Mihokova, A. Beitlerova, K. Bartosiewicz, S. Kurosawa, A. Yoshikawa, Defect engineering in Ce-doped aluminum garnet single crystal scintillators, Cryst. Growth Des. 14 (2014) 4827–4833. https://doi.org/10.1021/cg501005s.

[35] I. Gerasymov, S. Witkiewicz-Lukaszek, T. Zorenko, K. Bartosiewicz, Y. Zorenko, J. Winiecki, D. Kofanov, Y. Boyaryntseva, S. Tkachenko, P. Arhipov, E. Galenin, D. Kurtsev, O. Zelenskaya, V. Alekseev, K. Lebbou, O. Sidletskiy, Effects of codoping with divalent cations on performance of YAG:Ce,C scintillator, IEEE Trans. Nucl. Sci. 70 (2023) 1362–1369. https://doi.org/10.1109/tns.2023.3270320.

[36] A. Kilian, P. Bilski, V. Gorbenko, T. Zorenko, S. Witkiewicz, K. Paprocki, Y. Zorenko, Thermoluminescent properties of cerium-doped Lu_2SO_5 and Y_2SiO_5 single crystalline films scintillators grown from PbO-B_2O_3 and Bi_2O_3 fluxes, Crystals (Basel). 8 (2018) 120. https://doi.org/10.3390/cryst8030120.

[37] Y. Zorenko, V. Gorbenko, J. Vasylkiv, T. Strzyżewski, A. Fedorov, R. Kucerkova, J.A. Mares, M. Nikl, P. Bilski, A. Twardak, Growth and luminescent properties of scintillators based on the single crystalline films of $(Lu,Gd)_3(Al,Ga)_5O_{12}$:Ce garnets, J. Lumin. 169 (2016) 828–837. https://doi.org/10.1016/j.jlumin.2014.11.040.

[38] P.J. Yadav, C.P. Joshi, S.V. Moharil, One-step combustion synthesis of $Tb_3Al_5O_{12}$:Ce phosphor, Int. J. Self-Propagating High-Temp. Synth. 23 (2014) 41–46. https://doi.org/10.3103/s1061386214010117.

[39] M. Batentschuk, A. Osvet, G. Schierning, A. Klier, J. Schneider, A. Winnacker, Simultaneous excitation of Ce^{3+} and Eu^{3+} ions in $Tb_3Al_5O_{12}$, Radiat. Meas. 38 (2004) 539–543. https://doi.org/10.1016/j.radmeas.2003.12.009.